

Article

Battery-SOC Estimation for Hybrid-Power UAVs Using Fast-OCV Curve with Unscented Kalman Filters

Zhuoyao He ^{1,2,*}, David Martín Gómez ^{1,*} , Arturo de la Escalera Hueso ¹ , Pablo Flores Peña ³, Xingcai Lu ² and José María Armingol Moreno ¹ 

¹ Intelligent Systems Laboratory (LSI), Universidad Carlos III de Madrid, Av. Universidad 30, Leganés, 28911 Madrid, Spain; escalera@ing.uc3m.es (A.d.l.E.H.); armingol@ing.uc3m.es (J.M.A.M.)

² Key Laboratory for Power machinery and Engineering of M.O.E., Shanghai Jiao Tong University, Dongchuan Road No. 800, Shanghai 200240, China; lyuxc@sjtu.edu.cn

³ Drone Hopper S.L., Avenida Gregorio Peces-Barba, Leganés, 28919 Madrid, Spain; pablo.flores@drone-hopper.com

* Correspondence: zhuoyaohe@sjtu.edu.cn or zhuoyaohe@163.com (Z.H.); dmgoomez@ing.uc3m.es (D.M.G.)

Abstract: Unmanned aerial vehicles (UAVs) have drawn increasing attention in recent years, and they are widely applied. Nevertheless, they are generally limited by poor flight endurance because of the limited energy density of their batteries. A robust power supply is indispensable for advanced UAVs; thus hybrid power might be a promising solution. State of charge (SOC) estimation is essential for the power systems of UAVs. The limitations of accurate SOC estimation can be partly ascribed to the inaccuracy of open circuit voltage (OCV), which is obtained through specific forms of identification. Considering the actual operation of a battery under hybrid conditions, this paper proposes a novel method, “fast OCV”, for obtaining the OCVs of batteries. It is proven that fast OCV offers great advantages, related to its simplicity, duration and cost, over traditional ways of obtaining OCV. Moreover, fast-OCV also shows better accuracy in SOC estimation than traditional OCV. Furthermore, this paper also proposes a new method, “batch mode”, for talking-data sampling for battery-parameter identification with the limited-memory recursive least-square algorithm. Compared with traditional the “single mode”, it presents good de-noising effect by making use of all the sampled battery’s terminal current and voltage data.

Keywords: open-circuit voltage; state-of-charge estimation; battery-parameter identification; unscented Kalman filter; hybrid power; unmanned aerial vehicles



Citation: He, Z.; Martín Gómez, D.; de la Escalera Hueso, A.; Flores Peña, P.; Lu, X.; Armingol Moreno, J.M. Battery-SOC Estimation for Hybrid-Power UAVs Using Fast-OCV Curve with Unscented Kalman Filters. *Sensors* **2023**, *23*, 6429. <https://doi.org/10.3390/s23146429>

Academic Editors: Pasquale Daponte, Francesco Picariello and Francesco Lamonaca

Received: 16 June 2023
Revised: 9 July 2023
Accepted: 12 July 2023
Published: 15 July 2023



Copyright: © 2023 by the authors. Licensee MDPI, Basel, Switzerland. This article is an open access article distributed under the terms and conditions of the Creative Commons Attribution (CC BY) license (<https://creativecommons.org/licenses/by/4.0/>).

1. Introduction

As flying robots, UAVs are receiving increasing attention, with the advancement of microprocessor and artificial technologies [1]. Due to their advantages, such as their low cost and high mobility, UAVs are widely applied in numerous activities, like rescuing, monitoring, delivery, agriculture, and even military investigations, as well as battlefields [2–4], etc. However, the performances of UAVs are closely related to on-board power capabilities [5]. Generally, batteries are used as the main sources of power for UAVs; hence, the accurate assessment of the power states of batteries is extremely important for UAV missions [6,7].

The SOC, which means the charge available relative to the full charge capacity of a battery, is generally taken as a vital indicator for battery management [8,9]. Failures in SOC estimation can potentially lead to overcharging, over-discharging, or even irreversible damage to batteries [10]. However, the direct measurement of the SOC of a battery is not possible. In practical applications, indirect approaches are usually adopted for SOC estimation. Nevertheless, an accurate assessment of the SOC is usually of highly challenging, as it is complicated and associated with many factors [7,11], such as the charge-and-discharge efficiency, the charge-and-discharge rate, the temperature [12], etc. Thus far, various methods, like coulomb counting [13], artificial intelligence [14,15], the fuzzy logic algorithm,

and Kalman filters [16–18] have been widely investigated and used in SOC estimation. In comparison, the model-based method is relatively popular due to its simplicity [7,11]. Specifically, equivalent circuit models (ECM) combined with Kalman filters are the most popular, since they are widely adopted by numerous researchers.

As a function of SOC, the open-circuit voltage (OCV) is crucial for SOC estimation. It is usually used as a reference for innovation, which helps to improve the accuracy of state estimation for Kalman-filter-based SOC estimation. The crucial influence of the OCV on SOC estimation was disclosed in related studies through a large number of ECMs [19,20]. Currently, incremental OCV testing and low-current testing are usually used for OCV-curve abstraction [21,22]. However, such methods are usually time-consuming, owing to the battery-relaxation process. Furthermore, the complete measurement of OCV curves is not exclusive, as changes occur due to temperature and the battery's rate of aging [23–25]. Moreover, different batteries do not share the same OCV curve, even though they are from the same production line. All these factors indicate the strong necessity of efficient ways of obtaining OCV curves for batteries in practical applications.

To address these issues, several studies have been conducted by numerous researchers. Zhang et al. [26] proposed a non-experiment-based OCV-reconstruction method. However, it was mainly limited to a partial updating of an OCV curve. Fan et al. [27] introduced a method for efficiently reconstructing an OCV curve while considering the temperature variation of a battery by inspecting its charge-and-discharge process. Similarly, Cui et al. [28] conducted an OCV-curve reconstruction based on an electrode-OCV model; the results proved its effectiveness under different temperature conditions. However, these methods involved complex processes and struggled to meet time-efficiency requirements. Some other relevant studies were presented by many researchers [29–32] in recent years. Despite their significant achievements, these studies usually tried to establish possible ways of obtaining OCV curves as universally applicable. However, these methods do not offer positive solutions as specific conditions were not considered.

According to the idea of configuration, hybrid power systems that assemble engine/fuel cells and batteries can be classified as serial, parallel, or serial-parallel [33–35]. Regardless of the type, however, the engine/fuel cell is usually the primary power source, while the battery is an auxiliary part [36,37]. Regarding the application of hybrid power in UAVs, the battery can be better configured when it has a small capacity and, hence, light weight, as UAVs are weight-sensitive. Importantly, the ability to control charging and discharging of the battery can be achieved through the hybrid-powered UAV system, which is very similar to the core function of the professional battery-testing system. With this consideration, this paper aims to propose a fast and simple method for obtaining battery-OCV curves by making use of the configuration of the whole system. The obtained OCV curve is validated by conducting a SOC estimation for a battery with Kalman filters under different working conditions.

As previously stated, Kalman filters (KFs), extended Kalman filter (EKF), and unscented Kalman filters (UKFs), are the most popular approaches to SOC estimation. In terms of comparison, UKFs are drastically superior to KFs and EKFs when tackling non-linear systems due to their unscented transformation [38] and, hence, good robustness and high accuracy [39,40]. He et al. [41] conducted a comparative investigation of EKFs and UKFs for SOC estimation. The results showed that the UKF provided much better predictions. Zhang et al. [42] investigated a UKF for SOC estimation, and good predictions were obtained. Nevertheless, Kalman filters entail the predetermined covariance of the state and observation variables. However, these parameters are usually unknown and mainly set according to experiences. To overcome this drawback, in recent years, researchers have tended to adopt the Sage–Husa noise estimator for the online estimation of the covariance mentioned previously [43,44]. Combined with the noise estimator, an adaptive UKF (AUKF) was presented. Therefore, this paper attempts to validate an OCV curve obtained through battery-SOC estimations with UKF and AUKF.

The structure of this paper is as follows. In Section 2, we first discuss the ECM related to this work, and then the method of efficiently obtaining the OCV curve on the UAV with a hybrid power system is introduced theoretically and practically. In Section 3, the dynamic battery model and the AUKF specifically used in this research are discussed. In Section 4, the experiments involved in and the results of the method's validation are presented. Lastly, we draw conclusions in Section 5, in which we also discuss our expectations regarding future studies.

2. Model Selection, Testing Method, and Parameter Identification

2.1. Equivalent Circuit Models

To conduct a precise evaluation of battery characteristics, a robust model that describes the battery is essential. Numerous researchers have developed various models, which can generally be categorized into electrochemical models, neuro-network models, and equivalent circuit models (ECMs), among which ECMs are the most widely used owing to their simplicity and clear physical significance. In this paper, an ECM with n RC networks, which is called the n -order-polarization model, shown in Figure 1, is considered. Case n equals 1 (Thevenin model), is thoroughly involved in this investigation. However, case n equals 2 (dual polarization (DP) model) was also referred to during the model selection, while n equals 0 (Rint model) was used when obtaining the OCV.

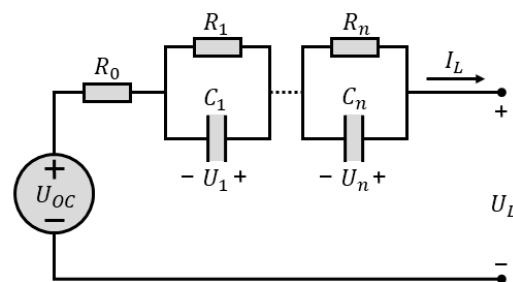


Figure 1. Schematic diagram of n -order polarization model.

With the advantage of calculation simplicity, Rint model is mainly applicable in situations with large currents, and transient characteristics are not considered. Thevenin model is constructed by using a parallel RC, which mimics the polarization effect of battery, in Rint model. Therefore, transient characteristics can be simulated. By introducing another parallel RC, which describes the diffusion effect of battery, to Thevenin mode, DP model is created. This model is usually able to describe the dynamic performance of a battery accurately.

2.2. Open-Circuit Voltage and Testing Method

For a precise SOC estimation, an OCV with relatively good accuracy is indispensable. Ordinarily, OCV can be observed by direct measurement after a sufficiently long time of rest for the battery. This method requires a significant amount of time to complete OCV observation. Many researchers conducted numerous investigations aiming at proposing potential universally applicable solutions. Examples include data-driven and model-driven solutions [31]. These methods may not always work when time efficiency and specific scenarios are considered. For battery in hybrid mode, online charging and discharging are naturally available. Considering the simplicity and applicability of OCV-construction method, specifically for battery in hybrid mode, this paper attempts to propose a simple method for OCV observation, as explained in the following content.

Take the simplest ECM, Rint model, into consideration and consider polynomial description of R_0 and OCV versus SOC, as shown in Equations (1) and (2). According to Figure 1, relationship between output voltage U_L and OCV can be formulated as Equation (3). The OCV equals U_L if I_L is set as 0; thus, OCV can be obtained if the coefficients in Equations (1) and (2) are solved. In fact, this can be easily achieved through

least-square method by collecting the charging/discharging data of the battery. For a better solution, charging and discharging were randomly shifted with a global discharging process for the test battery, which was initially fully charged. The current and voltage curves for the process mentioned here are shown in Figure 2.

$$R_0 = a_0 + a_1\text{SOC} + \dots + a_n\text{SOC}^n \quad (1)$$

$$\text{OCV} = b_0 + b_1\text{SOC} + \dots + b_n\text{SOC}^n \quad (2)$$

$$U_L = \text{OCV} - I_L R_0 \quad (3)$$

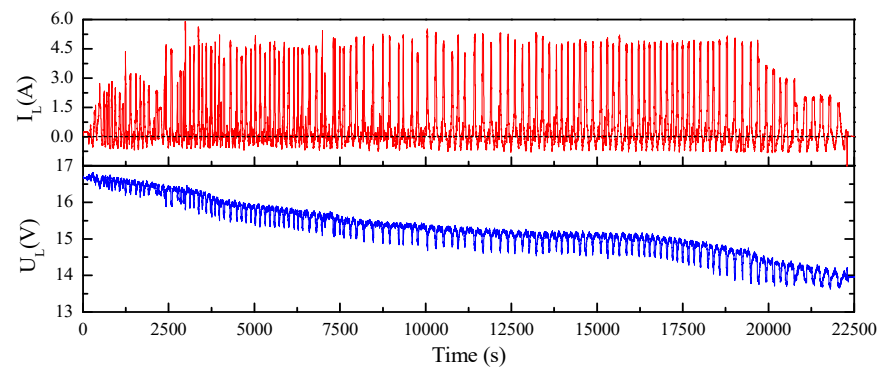


Figure 2. Charging-and-discharging process adopted in this paper.

However, to realize this process, as well as other tests, which are discussed below, a test set was created, as depicted in Figure 3. Battery was connected to motor propellers of UAV, while another power source with current controller was connected in parallel. Measurements of U_L and I_L focused on battery at point M. When setting current from fixed power-current controller, variations in the rotating speed of the motor propellers led to the variation of I_L in the battery.

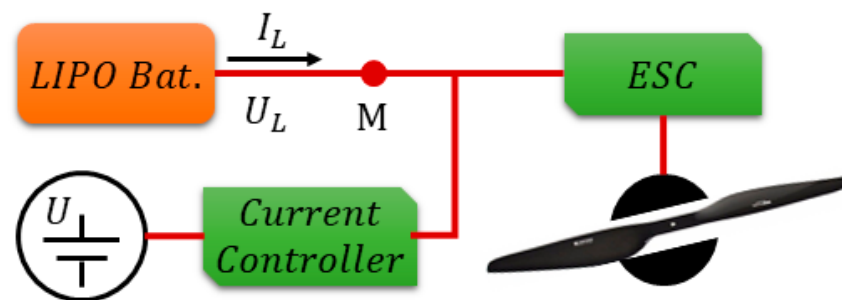


Figure 3. The method for realizing charging and discharging adopted in this paper.

For accurate current sensing, product LA 55-P/SP1, shown in Figure 4a, from LEM (Life Energy Motion) company was used. The principle of this transducer is shown in Figure 5a. When the primary current I_p (the target for measuring) passes through the coil, induced magnetic field is sensed by the Hall generator driven by current I_c with output of Hall voltage. This voltage is further sensed by closed-loop sensing circuit, which is mainly composed of an operational amplifier and a potential clamp. This closed-loop sensing circuit senses Hall voltage and drives the secondary current I_s to compensate the Hall voltage as zero. By sensing the voltage drop V_M on R_M , I_p is yielded. The I_p is forward when V_M is positive, and vice versa. The key parameters and measuring accuracy are shown in Tables 1–3.

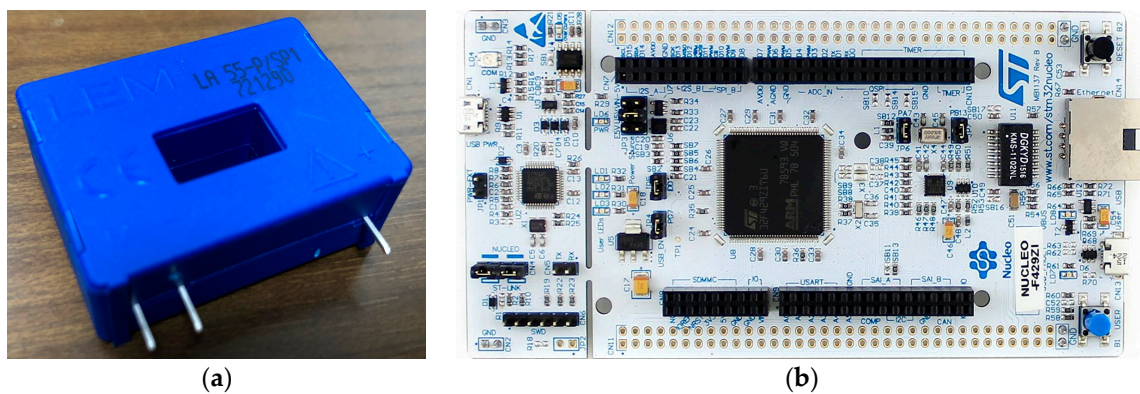


Figure 4. The key facilities used for signal sensing, testing-system control, and data sampling: (a) current transducer LA 55-P/SP1 used for current sensing; (b) STM32 Nucleo-144 boards F429ZI (MB1137) used for voltage sensing, data sampling, and system control.

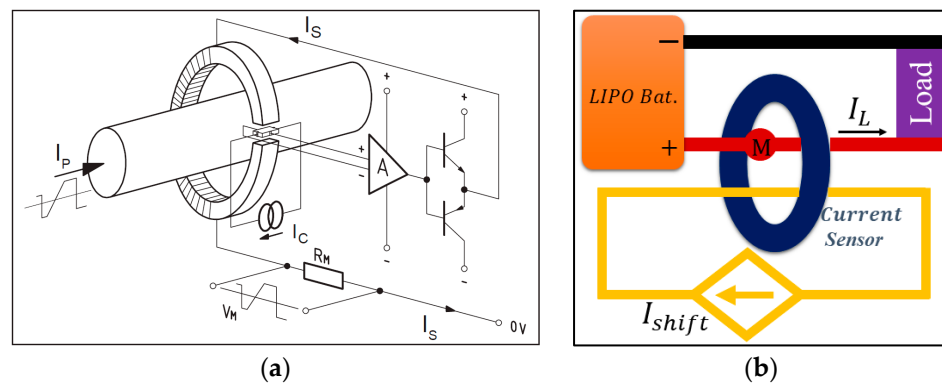


Figure 5. The method for sensing current reported in this paper: (a) operating principle of current transducer LA 55-P/SP1; (b) the method of current measurement with shift current in this paper.

Table 1. Key parameters of current transducer LA 55-P/SP1.

Primary Nominal RMS Current ($I_{p,N}$)	Primary Current Measuring Range ($I_{p,M}$)	Turns Ratio (N_p/N_s)	Supply Voltage ($\pm 5\%$) (U_C)
50 A	0~ ± 100 A	1:2000	$\pm 12\sim 15$ V

Table 2. Measurement-resistance requirements of current transducer LA 55-P/SP1.

Power Voltage	Measuring Resistance (R_M)			
	@TA = 70 °C		@TA = 85 °C	
	R_M Min	R_M Max	R_M Min	R_M Max
with ± 12 V	0 Ω	215 Ω	0 Ω	210 Ω
	0 Ω	35 Ω	0 Ω	30 Ω
with ± 15 V	0 Ω	335 Ω	30 Ω	330 Ω
	0 Ω	95 Ω	30 Ω	90 Ω

For controlling needs, STM32 Nucleo-144 boards, F429ZI (MB1137), were used to generate the driving signal fed to ESC. The Soc-STM32F429-embedded 12-bit ADC converter was mused to measure all the voltage signals. However, this ADC converter was not capable of converting negative voltage. Therefore, a constant current I_{shift} was fed across the current transducer, driving working state of the transducer to roughly the middle of positive measuring span when I_L equalled zero. By subtracting I_{shift} from the lumped measurement, I_L (either positive or negative) was yielded.

Table 3. Accuracy of parameters values of current transducer LA 55-P/SP1.

Error @ $I_p, T_A=25\text{ }^\circ\text{C}$		Linearity Error	Offset Current @ $I_p=0, T_A=25\text{ }^\circ\text{C}$	Delay Time @10% of $I_{p,N}$	Delay Time to 90% of $I_{p,N}$ ⁽¹⁾
@±15 V (±5%)	@±12~15 V (±5%)	<0.15%	within ±0.10 mA	<500 ns	<1 μs
±0.65%	±0.90%				

(1) For a $di/dt = 100\text{ A}/\mu\text{s}$.

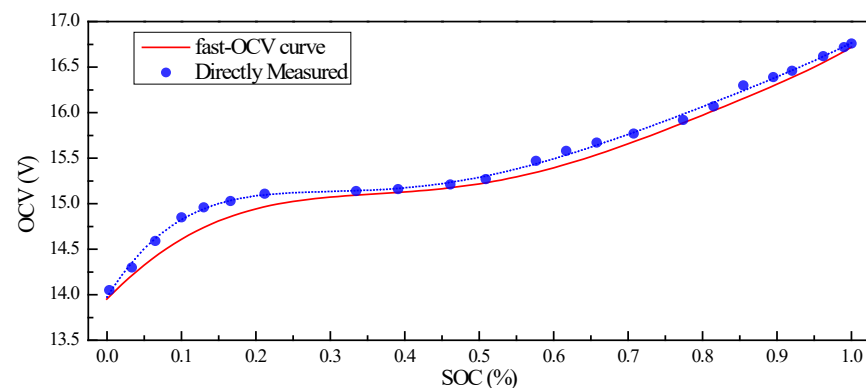
The sensing span of ADC converter on STM32F429 was between 0 V and 3 V. To measure the voltage signals exceeding this range, voltage-divider circuit composed of resistor was applied for signal conversion. However, considering the accuracy of the circuit, RS PRO Mini AC/DC Clamp (Stock No. 146-9096) was used for calibration of voltage-signal measurement.

In this paper, 6-order polynomial was adopted for Equations (1) and (2). Basic information on the battery and the coefficients solved is shown in Table 4. For comparison, OCV derived through traditional measurement is also included in this paper, as shown in Figure 6.

Table 4. Battery information and coefficients of R_0 and OCV polynomials.

Coefficient	Value	Coefficient	Value	Coefficient	Value
a_0	0.18178	a_1	−0.92811	a_2	3.6568
a_3	−6.8357	a_4	5.9269	a_5	−1.7057
a_6	−0.22173	b_0	13.951	b_1	8.3961
b_2	−18.459	b_3	−4.6272	b_4	69.866
b_5	−82.283	b_6	29.877		

Battery information: Lipo, 4S1P, 14.8V,45C

**Figure 6.** OCV obtained through direct measurement and dynamic current experiments (fast OCV) described in this paper.

2.3. Parameter Identification

In this paper, we consider Thevenin model and DP model for battery description. However, before SOC estimation, R_i and C_i in the model should be identified. This paper uses limited-memory recursive least-square algorithm to achieve parameter identification.

Consider DP model of battery. Time-related relationship between $U_{OC}(t)$, $I_L(t)$, $U_1(t)$ and $U_2(t)$ can be described with Equations (4)–(6).

$$U_{OC}(t) = I_L(t)R_0 + U_1(t) + U_2(t) + U_L(t) \quad (4)$$

$$I_L(t) = U_1(t)/R_1 + C_1 dU_1(t)/dt \quad (5)$$

$$I_L(t) = U_2(t)/R_2 + C_2 dU_2(t)/dt \tag{6}$$

After Laplace transformation, Equations (7)–(9) can be obtained.

$$U_{OC}(s) = I_L(s)R_0(s) + U_1(s) + U_2(s) + U_L(s) \tag{7}$$

$$I_L(s) = U_1(s)/R_1 + C_1 sU_1(s) \tag{8}$$

$$I_L(s) = U_2(s)/R_2 + C_2 sU_2(s) \tag{9}$$

With a summary of Equations (7)–(9), the relationship between $U_{OC}(t)$, $I_L(t)$, $U_1(t)$ and $U_2(t)$ can be described by Equation (10).

The definitions of a , b , c , d , and e are shown in Equation set (11), where τ_1 and τ_2 signify R_1C_1 and R_2C_2 .

$$(1 + as + bs^2)U_{OC}(s) = (c + es + ds^2)I_L(s) + (1 + as + bs^2)U_L(s) \tag{10}$$

$$\begin{cases} a = \tau_1 + \tau_2 \\ b = \tau_1\tau_2 \\ c = R_0 + R_1 + R_2 \\ d = \tau_1\tau_2R_0 \\ e = (\tau_1 + \tau_2)R_0 + \tau_1R_2 + \tau_2R_1 \end{cases} \tag{11}$$

By identifying a , b , c , d , and e in Equation set (11), parameters R_0 , R_1 , C_1 , R_2 , and C_2 can be determined. To achieve this, Equation (10) is transformed into (12) through inverse Laplace transformation.

$$U_{OC}(t) + a \frac{dU_{OC}(t)}{dt} + b \frac{d^2U_{OC}(t)}{dt^2} = cI_L(t) + d \frac{dI_L(t)}{dt} + e \frac{d^2I_L(t)}{dt^2} + U_L + a \frac{dU_L(t)}{dt} + b \frac{d^2U_L(t)}{dt^2} \tag{12}$$

Discretization can then be applied to (12). In this investigation, the current from the battery is small in relation to relatively high capacity of the battery; thus derivative terms $dU_{OC}(t)/dt$ and $d^2U_{OC}(t)/dt^2$ are negligible and, hence, ignored.

$$w_0 + w_1I_t + w_2I_{t-T} + w_3I_{t-2T} + w_4U_{L,t-T} + w_5U_{L,t-2T} = U_{L,t} \tag{13}$$

$$\begin{cases} w_0 = T^2U_{OC,t}/M \\ w_1 = -(cT^2 + eT + d)/M \\ w_2 = (eT + 2d)/M \\ w_3 = -d/M \\ w_4 = (aT + 2b)/M \\ w_5 = -b/M \end{cases} \tag{14}$$

Let $M = T^2 + aT + b$, where T is the refresh-time interval. The discretized formation of (12) is obtained as (13). Coefficients $w_0 \sim w_5$ can be expressed by coefficients $a \sim e$ through Equation set (14). By solving Equation (13), $w_0 \sim w_5$ can be determined, and $a \sim e$, R_0 , R_1 , C_1 , and R_2 , and C_2 can be obtained.

$$X_{t,i} = (1, I_{t-ih}, I_{t-T-ih}, I_{t-2T-ih}, U_{L,t-T-ih}, U_{L,t-2T-ih}) \tag{15}$$

$$Y_{t,i} = (U_{L,t-ih}) \tag{16}$$

$$W_t = (w_{0,t}, w_{1,t}, w_{2,t}, w_{3,t}, w_{4,t}, w_{5,t})^T \quad (17)$$

$$\begin{cases} K_t = P_{t-T} X_t^T (\alpha E + X_t P_{t-T} X_t^T)^{-1} \\ P_t = (E - K_t X_t) P_{t-T} / \alpha \\ W_t = W_{t-1} + K_t (Y_t - X_t W_{t-1}) \end{cases} \quad (18)$$

$$P_0 = (X_0^T X)^{-1} \quad (19)$$

$$W_0 = P_0 X_0^T Y_0 \quad (20)$$

In this paper, limited-memory recursive least squares is used to solve the equation to avoid data saturation. The α is set as 0.99. To initiate the algorithm, a set of data are used to give reasonable initial value for P and W through Equations (19) and (20).

All above are related to DP model. However, the deduction of algorithm for Thevenin model is very similar; hence, it is omitted for simplicity.

The method for creating X_t and Y_t is shown in Figure 7. In the experiments, sample time h was 0.064 s, and a calculation was conducted every 20 times on each sample, i.e., refresh time $T = 20 \times h = 1.28$ s; thus, the estimated parameters were refreshed. In fact, limited-memory recursive least squares is mainly used for online calculations. Thus, X_t usually only contains one sample to precipitate the calculation process. We call it “single mode” here. In contrast, case X_t contains more than one sample. Here, it is called “batch mode”. The X_t contains 20 samples with batch mode in this investigation.

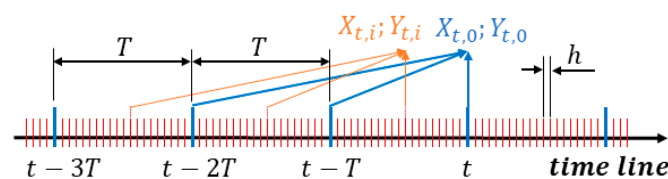


Figure 7. Explanation of $X_{t,i}$ $Y_{t,i}$; sample time h and refresh time T .

For DP model, parameter estimation involves solving quadratic equation. Specifically, $\Delta = a^2 - 4b$ should be non-negative; thus a real solution for the parameters can be realized. However, results proved that Δ value for the test was always negative, which means that DP model is not suitable for the battery in this research. Thus, Thevenin model is adopted in the following discussion (Figure 8).

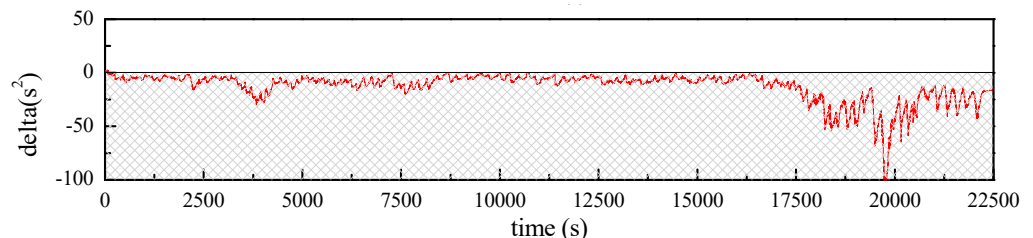


Figure 8. Values of Δ during the entire test.

As shown in Figure 9, parameters R_0 , R_1 , and C_1 are successfully estimated and batch mode is obviously superior to single mode in terms of prediction stability. By tracking SOC of the battery, a lookup table of R_0 , R_1 , and C_1 versus SOC was developed for SOC estimation under working conditions.

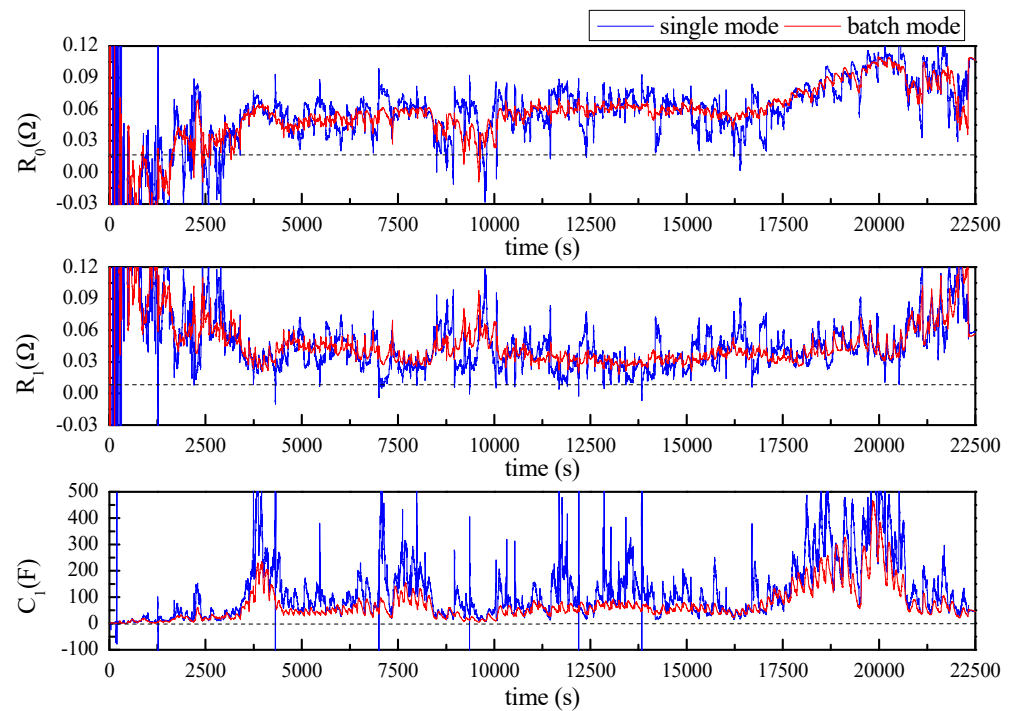


Figure 9. Estimated parameters R_0 , R_1 , and C_1 with Thevenin model.

3. AUKF for SOC Estimation

3.1. State Equation and Observation Equation for Thevenin Battery Model

According to the Thevenin model, it is obvious that the U_{OC} or SOC and U_1 can be selected as the complete state variables for the battery. For convenience, we consider SOC instead of U_{OC} to avoid a conversion from U_{OC} to SOC when making predictions. Therefore, the state-transfer equation can be expressed as (23), where ε_t is the process-noise vector.

$$SOC_t = SOC_0 - \int_0^t \eta I_\tau d\tau / C_a \quad (21)$$

$$U_{1,t} = (1 - T/\tau_1)U_{1,t-T} + TI_t/C_1 \quad (22)$$

$$\begin{bmatrix} SOC_t \\ U_{1,t} \end{bmatrix} = \begin{bmatrix} 1 & 0 \\ 0 & 1 - \frac{T}{\tau_1} \end{bmatrix} \begin{bmatrix} SOC_{t-T} \\ U_{1,t-T} \end{bmatrix} + \begin{bmatrix} -\frac{\eta T}{C_a} \\ \frac{T}{C_1} \end{bmatrix} I_t + \varepsilon_t \quad (23)$$

The SOC_t value from the initial value of the SOC_0 by the actuation of current I_t can be expressed as Equation (21), where η is the charging efficiency and C_a is the capacity of the battery. The effect of the actuation I_t on U_1 can be expressed as Equation (22). Therefore, the state-transfer equation can be expressed as

$$U_{L,t} = U_{OC}(SOC_t) - U_{1,t} - R_0 I_t + \delta_t \quad (24)$$

Similarly, the observation equation can be expressed as (24), where δ_t is the observation noise.

Let $x_t = [SOC_t \quad U_{1,t}]^T$, $u_t = I_t$, $y_t = U_{L,t}$. The standard form of the dynamic battery system's description can be obtained as shown in Equation (25).

$$\begin{cases} x_t = f(x_{t-1}, I_t) + \varepsilon_t \\ y_t = g(x_t, I_t) + \delta_t \end{cases} \quad (25)$$

3.2. Adaptive Unscented Kalman Filter

Assuming that the process noise and observation noise are uncorrelated white Gaussian noise, i.e., $\varepsilon_t \sim N(0, R_t)$, $\delta_t \sim N(0, Q_t)$, The standard UKF algorithm is as follows:

(1) State value and covariance initialization:

$$\begin{cases} \bar{x}_0 = E(x_0) \\ \Sigma_0 = E[(x_0 - \bar{x}_0)(x_0 - \bar{x}_0)^T] \end{cases} \quad (26)$$

(2) Sigma-point generation:

$$\begin{cases} \mathcal{L}_{t-1}^{[0]} = x_{t-1} \\ \mathcal{L}_{t-1}^{[i]} = x_{t-1} + \gamma(\sqrt{\Sigma_{t-1}})_i, i = 1, 2, \dots, n \\ \mathcal{L}_{t-1}^{[i+n]} = x_{t-1} - \gamma(\sqrt{\Sigma_{t-1}})_i, i = 1, 2, \dots, n \end{cases} \quad (27)$$

where $\gamma = \sqrt{\lambda + n}$, $\lambda = \alpha^2(n + k) - n$. The parameters α and k are used to determine how far all the sigma points are distributed from the mean value. In this research, α and k are set as 1 and 0, respectively.

(3) Coefficient calculation:

$$\begin{cases} \omega_m^{[0]} = \frac{\lambda}{\lambda + n} \\ \omega_c^{[0]} = \frac{\lambda}{\lambda + n} + (1 - \alpha^2 + \beta) \\ \omega_m^{[i]} = \omega_c^{[i]} = \frac{1}{2(n + \lambda)}, i = 1, 2, \dots, n \end{cases} \quad (28)$$

In fact, both $\omega_m^{[i]}$ and $\omega_c^{[i]}$ correspond to one sigma point, $\mathcal{L}_{t-1}^{[i]}$, while $\omega_m^{[i]}$ is used for the mean value calculation and $\omega_c^{[i]}$ is used for the covariance calculation. Parameter β should be set as 2 for Gaussian distribution, which is the case in this investigation.

(4) Process update for sigma points and covariance:

$$\bar{\mathcal{L}}_t^{*[i]} = f(\mathcal{L}_{t-1}^{[i]}, I_t) \quad (29)$$

$$\bar{x}_t = \sum_{i=0}^{2n} \omega_m^{[i]} \bar{\mathcal{L}}_t^{*[i]} \quad (30)$$

$$\bar{\Sigma}_t = \sum_{i=0}^{2n} \omega_c^{[i]} (\bar{\mathcal{L}}_t^{*[i]} - \bar{x}_t) (\bar{\mathcal{L}}_t^{*[i]} - \bar{x}_t)^T + R_t \quad (31)$$

(5) Kalman-gain calculation:

$$\begin{cases} \bar{\mathcal{L}}_t^{[0]} = \bar{x}_t \\ \bar{\mathcal{L}}_t^{[i]} = \bar{x}_t + \gamma(\sqrt{\bar{\Sigma}_t})_i, i = 1, 2, \dots, n \\ \bar{\mathcal{L}}_t^{[i+n]} = \bar{x}_t - \gamma(\sqrt{\bar{\Sigma}_t})_i, i = 1, 2, \dots, n \end{cases} \quad (32)$$

$$\bar{y}_t^{[i]} = g(\bar{\mathcal{L}}_t^{[i]}, I_t) \quad (33)$$

$$\hat{y}_t = \sum_{i=0}^{2n} \omega_m^{[i]} \bar{y}_t^{[i]} \quad (34)$$

$$S_t = \sum_{i=0}^{2n} \omega_c^{[i]} (\bar{y}_t^{[i]} - \hat{y}_t) (\bar{y}_t^{[i]} - \hat{y}_t)^T + Q_t \quad (35)$$

$$\bar{\Sigma}_t^{x,y} = \sum_{i=0}^{2n} \omega_c^{[i]} (\bar{\mathcal{L}}_t^{[i]} - \bar{x}_t) (\bar{\mathcal{L}}_t^{[i]} - \bar{x}_t)^T \quad (36)$$

$$K_t = \bar{\Sigma}_t^{x,y} S_t^{-1} \quad (37)$$

(6) State and covariance update:

$$e_t = z_t - \hat{y}_t \quad (38)$$

$$x_t = \bar{x}_t + K_t e_t \quad (39)$$

$$\Sigma_t = \bar{\Sigma}_t - K_t S_t K_t^T \quad (40)$$

(7) Adaptive noise estimation:

$$D_t = e_t e_t^T \quad (41)$$

$$R_{t+1} = (1 - d_t) R_t + d_t K_t D_t K_t^T \quad (42)$$

$$Q_{t+1} = (1 - d_t) Q_t + d_t \left(\sum_{i=0}^{2n} \omega_c^{[i]} (\bar{y}_t^{[i]} - \hat{y}_t) (\bar{y}_t^{[i]} - \hat{y}_t)^T + D_t \right) \quad (43)$$

where d_t is expressed as

$$d_t = \frac{1 - b}{1 - b^{t+1}}, \quad (0 < b < 1) \quad (44)$$

where b is the forgetting factor and was set as 0.95 in this study.

4. Experiments, Results, and Discussion

To establish the performance of the application of the fast-OCV in the SOC estimation, two working conditions, continuous discharge and step discharge, as shown in Figures 10 and 11, were tested. Furthermore, UKF and AUKF algorithms were adopted for the comparative investigations.

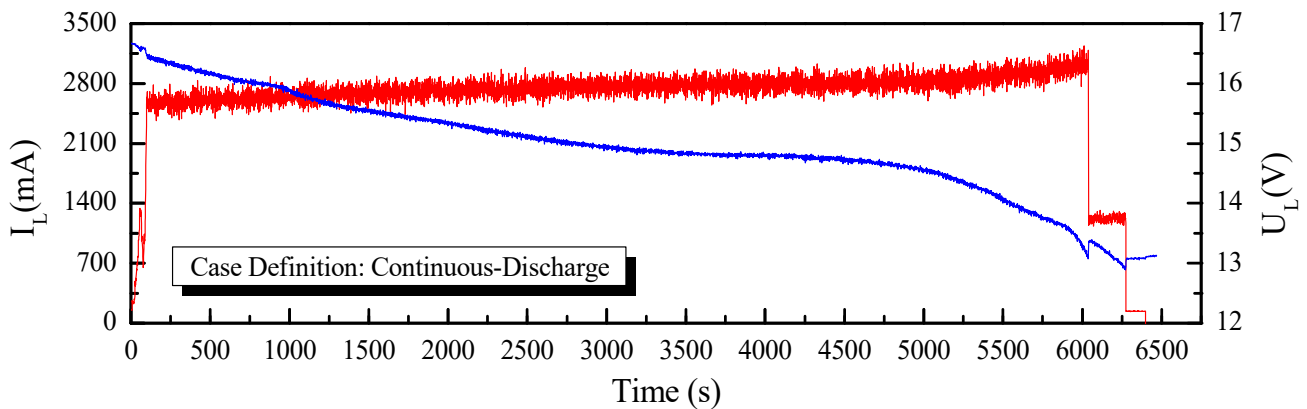


Figure 10. Current and voltage curves for continuous-discharge case.

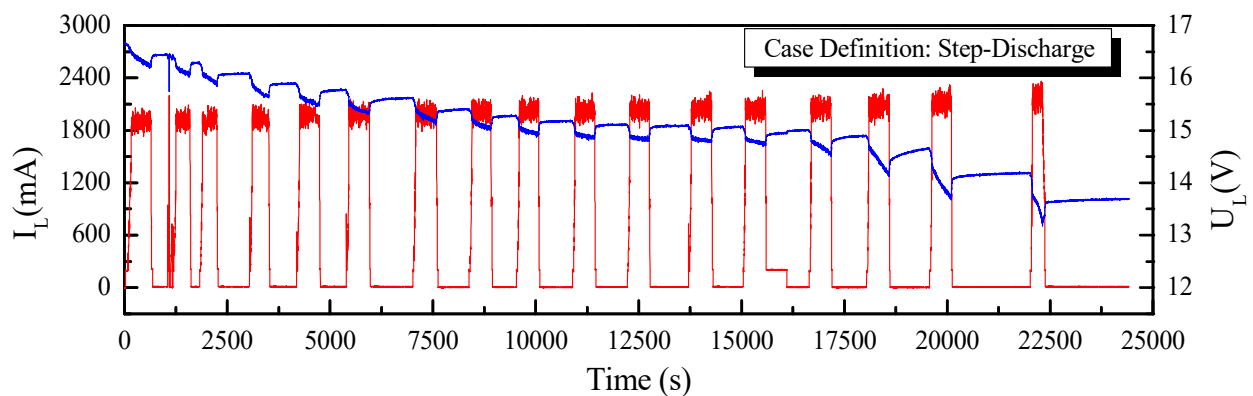


Figure 11. Current and voltage curves for step-discharge case.

The initial value SOC_0 was set as 0.2, which was obviously not the real value, to establish how quickly each case converged with the real value. As shown in Figures 12 and 13, all the predictions followed the trend of the SOC variation. However, we found that the fast OCV showed an obviously better accuracy. Furthermore, the fast OCV cases also showed faster convergence. This might have been due to the fact that the fast OCV was obtained under real application conditions, which are closer to actual working conditions than traditional ways of obtaining the OCV. However, all the cases lost track with the actual SOC when the battery was about to become empty. This phenomenon would possibly be ascribed to the drawback that the Thevenin model does not describe the diffusion effect, or to the fact that there was a lack of optimization on the current trace when carrying out the parameter identification.

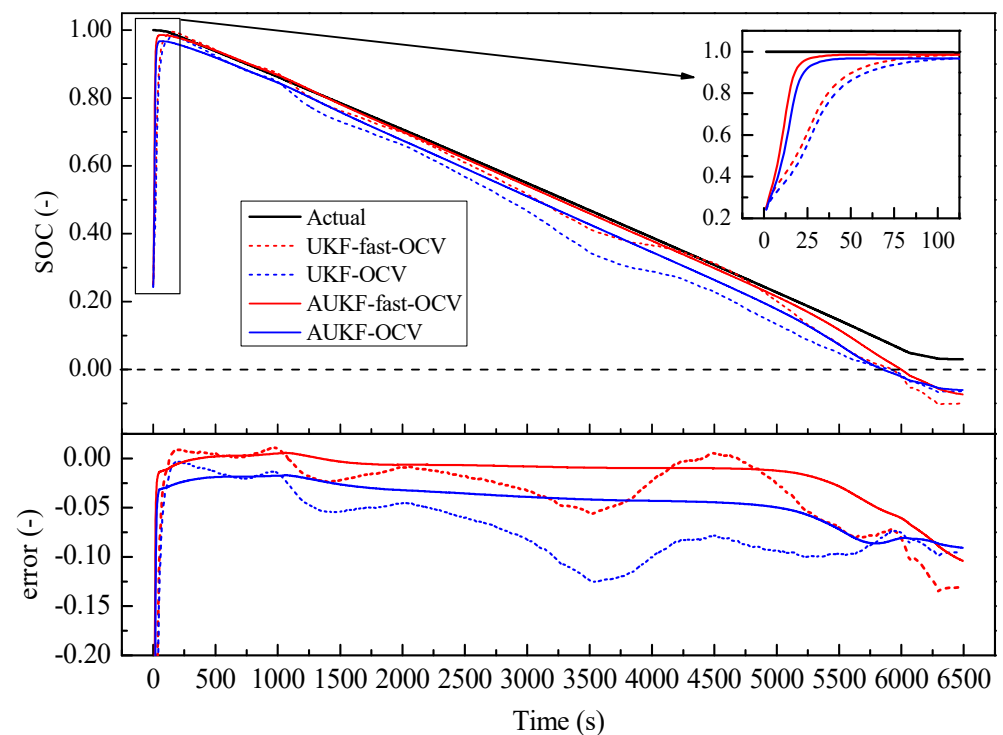


Figure 12. Comparison of SOC estimation: fast OCV versus traditional OCV under continuous-discharge condition.

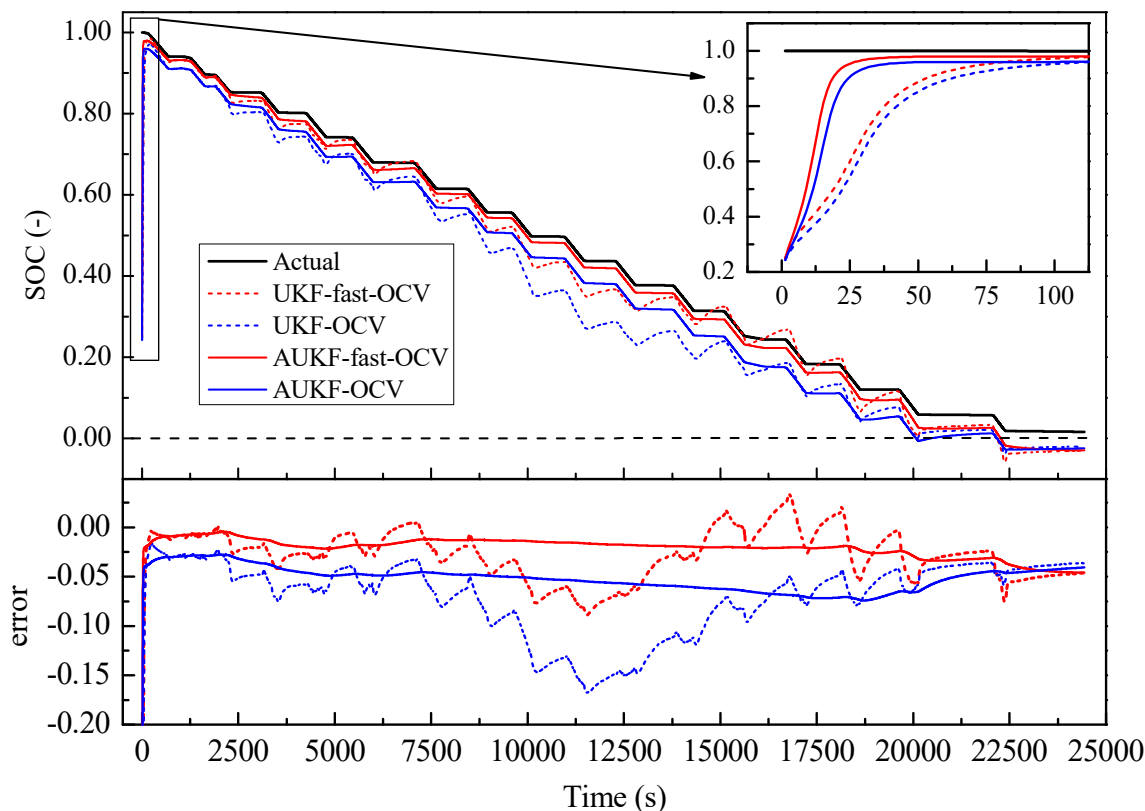


Figure 13. Comparison of SOC estimations: fast OCV versus traditional OCV under step-discharge conditions.

According to the results shown in Figures 12 and 13, it was also found that the AUKF showed a much better performance than the UKF. For the classical UKF, the covariance for the process noise and observation noise might not be optimal. However, with the adaptive estimation of the noise covariance, the Kalman filter worked more closely to the optimum performance; hence, the AUKF showed much better performances. It was also found in both cases that relatively large errors resulted when the SOC was low. This was mainly due to the fact that the OCV curve was obtained based on the Rint model. However, in the low-SOC situation, a distinct relaxation effect was observed, which was confirmed by the relatively large R_1 and C_1 values shown in Figure 9. Nevertheless, good accuracy in the SOC estimation was achieved within a large SOC span by using the fast-OCV curve with the AUKF algorithm.

All the results showed that the fast OCV exhibited very good performances when used for SOC estimation. These results seem to be unreasonable, as we observed that the fast OCV obviously deviated from the measured value, as shown in Figure 6. However, the ECM here was largely simplified, meaning that it may not have been able to describe the battery's behavior in significant detail; thus, the OCV curve was not necessarily very close to the real value, but it was more compatible with the model [25]. In our case, the battery was described with the Thevenin model. The OCV was obtained with the assumption of the Rint model, which is of similar simplicity to the Thevenin model; hence, good compatibility was achieved between the OCV curve and the ECM. However, there are still some deficiencies in this method, specifically when the SOC is low, which suggests that poor compatibility between the OCV and ECM might be encountered. Therefore, more thorough work is still required in future investigations. When carrying out the parameter estimations with the limited-memory least-square algorithm, the batch mode showed much weaker noise. Considering the Kalman filters in this work, the performance in the parameter estimation might be further improved in further investigations in the future.

5. Conclusions

In this paper, the fast-OCV method was used to obtain the open-circuit voltage of a battery. By using Kalman filters, the battery SOC was estimated. To obtain the battery parameters, the dynamic battery model was discretized to form a linear equation for parameter solution by using the sampled terminal current and voltage data. To minimize data noise, a “batch mode” method was introduced to sufficiently use all the sampled data obtained with high frequency. Moreover, the limited-memory recursive least-square algorithm was used to smooth the solution. The main conclusions of this research are as follows:

- (1) The “batch-mode” proposed was able to make good use of all the data sampled, with a much higher frequency than the parameter-updating task, and it demonstrated a good de-noising effect in the battery-parameter estimation. Combined with the limited-memory recursive least-square algorithm, successful parameter estimation was achieved.
- (2) The fast-OCV curve based on the Rint model was applied effectively for battery-SOC estimation. Compared with the traditionally obtained OCV curve, it even proved to offer much better accuracy in SOC estimation. Combined with an adaptive UKF, good accuracy in SOC estimation was achieved.
- (3) Compared with the traditional approach to OCV curve identification, the fast-OCV method is much more time-efficient, with a completely fluctuating charging-and-discharging process. As hybrid power for UAVs should be configured with low capacity (light batteries), the fast-OCV method is highly suitable for these situations.

Nevertheless, the results also showed the relatively poor accuracy of the proposed method in SOC estimation in low-SOC situations. This was probably mainly due to the higher relaxation effect when the SOC was low, as indicated by the relatively high R_1 and C_1 values. To perfect the OCV-curve identification, a first- or second-order ECM may need to be considered. Furthermore, the approach to fluctuating the current load on the battery may also affect the results of OCV curve obtained. The investigation of this topic would involve standard waves, like sinusoid waves and rectangular waves, or even standard battery-testing cycles. All these points are worthy of future investigations.

Author Contributions: Conceptualization, Z.H.; methodology, Z.H. and D.M.G.; software, Z.H.; validation, Z.H. and D.M.G.; formal analysis, Z.H. and D.M.G.; investigation, Z.H.; resources, J.M.A.M., A.d.I.E.H., D.M.G. and P.F.P.; data curation, Z.H.; writing—original draft preparation, Z.H.; writing—review and editing, Z.H. and D.M.G.; visualization, Z.H.; supervision, D.M.G.; project administration, J.M.A.M., P.F.P. and D.M.G.; funding acquisition, Z.H., D.M.G., J.M.A.M. and X.L. All authors have read and agreed to the published version of the manuscript.

Funding: This research was funded by Spanish Government, grant number PID2019-104793RB-C31 and PID2021-124335OB-C21; Comunidad de Madrid, grant number SEGVAUTO-4.0-CM (P2018/EMT-4362); and National Natural Science Foundation of China, grant number 52236007 and 52106176.

Institutional Review Board Statement: Not applicable.

Informed Consent Statement: Not applicable.

Data Availability Statement: Not applicable.

Conflicts of Interest: The authors declare no conflict of interest.

References

1. Adnan, N.; Nordin, S.M.; bin Bahruddin, M.A. Sustainable interdependent networks from smart autonomous vehicle to intelligent transportation networks. In *Sustainable Interdependent Networks II: From Smart Power Grids to Intelligent Transportation Networks*; Springer: Berlin/Heidelberg, Germany, 2019; pp. 121–134.
2. Yang, T.; Jiang, Z.; Sun, R.; Cheng, N.; Feng, H. Maritime search and rescue based on group mobile computing for unmanned aerial vehicles and unmanned surface vehicles. *IEEE Trans. Ind. Inform.* **2020**, *16*, 7700–7708. [[CrossRef](#)]
3. Kim, J.; Kim, S.; Ju, C.; Son, H.I. Unmanned aerial vehicles in agriculture: A review of perspective of platform, control, and applications. *IEEE Access* **2019**, *7*, 105100–105115. [[CrossRef](#)]

4. Wan, P.; Hao, B.; Li, Z.; Ma, X.; Zhao, Y. Accurate estimation the scanning cycle of the reconnaissance radar based on a single unmanned aerial vehicle. *IEEE Access* **2017**, *5*, 22871–22879. [[CrossRef](#)]
5. Jaeger, M.; Adair, D. Conceptual design of a high-endurance hybrid electric unmanned aerial vehicle. *Mater. Today Proc.* **2017**, *4*, 4458–4468. [[CrossRef](#)]
6. De Sutter, L.; Firouz, Y.; De Hoog, J.; Omar, N.; Van Mierlo, J. Battery aging assessment and parametric study of lithium-ion batteries by means of a fractional differential model. *Electrochim. Acta* **2019**, *305*, 24–36. [[CrossRef](#)]
7. Hannan, M.A.; Lipu, M.H.; Hussain, A.; Mohamed, A. A review of lithium-ion battery state of charge estimation and management system in electric vehicle applications: Challenges and recommendations. *Renew. Sustain. Energy Rev.* **2017**, *78*, 834–854. [[CrossRef](#)]
8. Noura, N.; Boulon, L.; Jemeï, S. A review of battery state of health estimation methods: Hybrid electric vehicle challenges. *World Electr. Veh. J.* **2020**, *11*, 66. [[CrossRef](#)]
9. Rivera-Barrera, J.P.; Muñoz-Galeano, N.; Sarmiento-Maldonado, H.O. SoC estimation for lithium-ion batteries: Review and future challenges. *Electronics* **2017**, *6*, 102. [[CrossRef](#)]
10. Partovibakhsh, M.; Liu, G. An adaptive unscented Kalman filtering approach for online estimation of model parameters and state-of-charge of lithium-ion batteries for autonomous mobile robots. *IEEE Trans. Control Syst. Technol.* **2014**, *23*, 357–363. [[CrossRef](#)]
11. How, D.N.; Hannan, M.; Lipu, M.H.; Ker, P.J. State of charge estimation for lithium-ion batteries using model-based and data-driven methods: A review. *IEEE Access* **2019**, *7*, 136116–136136. [[CrossRef](#)]
12. Zhang, R.; Li, X.; Sun, C.; Yang, S.; Tian, Y.; Tian, J. State of Charge and Temperature Joint Estimation Based on Ultrasonic Reflection Waves for Lithium-Ion Battery Applications. *Batteries* **2023**, *9*, 335. [[CrossRef](#)]
13. Ng, K.S.; Moo, C.-S.; Chen, Y.-P.; Hsieh, Y.-C. Enhanced coulomb counting method for estimating state-of-charge and state-of-health of lithium-ion batteries. *Appl. Energy* **2009**, *86*, 1506–1511. [[CrossRef](#)]
14. Theiler, M.; Schneider, D.; Endisch, C. Kalman Filter Tuning Using Multi-Objective Genetic Algorithm for State and Parameter Estimation of Lithium-Ion Cells. *Batteries* **2022**, *8*, 104. [[CrossRef](#)]
15. Vidal, C.; Malysz, P.; Kollmeyer, P.; Emadi, A. Machine learning applied to electrified vehicle battery state of charge and state of health estimation: State-of-the-art. *IEEE Access* **2020**, *8*, 52796–52814. [[CrossRef](#)]
16. Deng, Z.; Yang, L.; Cai, Y.; Deng, H. Online identification with reliability criterion and state of charge estimation based on a fuzzy adaptive extended Kalman filter for lithium-ion batteries. *Energies* **2016**, *9*, 472. [[CrossRef](#)]
17. Li, J.; Ye, M.; Jiao, S.; Meng, W.; Xu, X. A novel state estimation approach based on adaptive unscented Kalman filter for electric vehicles. *IEEE Access* **2020**, *8*, 185629–185637. [[CrossRef](#)]
18. Peng, S.; Chen, C.; Shi, H.; Yao, Z. State of charge estimation of battery energy storage systems based on adaptive unscented Kalman filter with a noise statistics estimator. *IEEE Access* **2017**, *5*, 13202–13212. [[CrossRef](#)]
19. Yu, Q.-Q.; Xiong, R.; Wang, L.-Y.; Lin, C. A comparative study on open circuit voltage models for lithium-ion batteries. *Chin. J. Mech. Eng.* **2018**, *31*, 65. [[CrossRef](#)]
20. Zheng, Y.; Ouyang, M.; Han, X.; Lu, L.; Li, J. Investigating the error sources of the online state of charge estimation methods for lithium-ion batteries in electric vehicles. *J. Power Sources* **2018**, *377*, 161–188. [[CrossRef](#)]
21. Chen, Z.; Fu, Y.; Mi, C.C. State of charge estimation of lithium-ion batteries in electric drive vehicles using extended Kalman filtering. *IEEE Trans. Veh. Technol.* **2012**, *62*, 1020–1030. [[CrossRef](#)]
22. Weng, C.; Sun, J.; Peng, H. A unified open-circuit-voltage model of lithium-ion batteries for state-of-charge estimation and state-of-health monitoring. *J. Power Sources* **2014**, *258*, 228–237. [[CrossRef](#)]
23. Lin, C.; Yu, Q.; Xiong, R. A study on the impact of open circuit voltage tests on state of charge estimation for lithium-ion batteries. *Appl. Energy* **2017**, *205*, 892–902. [[CrossRef](#)]
24. Campestrini, C.; Kosch, S.; Jossen, A. Influence of change in open circuit voltage on the state of charge estimation with an extended Kalman filter. *J. Energy Storage* **2017**, *12*, 149–156. [[CrossRef](#)]
25. Farmann, A.; Sauer, D.U. A study on the dependency of the open-circuit voltage on temperature and actual aging state of lithium-ion batteries. *J. Power Sources* **2017**, *347*, 1–13. [[CrossRef](#)]
26. Zhang, S.; Zhang, X. A novel non-experiment-based reconstruction method for the relationship between open-circuit-voltage and state-of-charge/state-of-energy of lithium-ion battery. *Electrochim. Acta* **2022**, *403*, 139637. [[CrossRef](#)]
27. Fan, K.; Wan, Y.; Wang, Z.; Jiang, K. Time-efficient identification of lithium-ion battery temperature-dependent OCV-SOC curve using multi-output Gaussian process. *Energy* **2023**, *268*, 126724. [[CrossRef](#)]
28. Cui, Z.; Cui, N.; Li, C.; Lu, J.; Zhang, C. Online Identification and Reconstruction of Open-Circuit Voltage for Capacity and Electrode Aging Estimation of Lithium-Ion Batteries. *IEEE Trans. Ind. Electron.* **2023**, *70*, 4716–4726. [[CrossRef](#)]
29. Tian, J.; Xiong, R.; Shen, W.; Sun, F. Electrode ageing estimation and open circuit voltage reconstruction for lithium ion batteries. *Energy Storage Mater.* **2021**, *37*, 283–295. [[CrossRef](#)]
30. Xu, X.; Xu, Z.; Wang, T.; Xu, J.; Pei, L. Open-circuit voltage curve reconstruction for degrading lithium-ion batteries utilizing discrete curve fragments from an online dataset. *J. Energy Storage* **2022**, *56*, 106003. [[CrossRef](#)]
31. Wang, Y.; Cheng, Y.; Xiong, Y.; Yan, Q. Estimation of battery open-circuit voltage and state of charge based on dynamic matrix control-extended Kalman filter algorithm. *J. Energy Storage* **2022**, *52*, 104860. [[CrossRef](#)]

32. Chen, X.; Lei, H.; Xiong, R.; Shen, W.; Yang, R. A novel approach to reconstruct open circuit voltage for state of charge estimation of lithium ion batteries in electric vehicles. *Appl. Energy* **2019**, *255*, 113758. [[CrossRef](#)]
33. Yang, X.; Pei, X. Hybrid system for powering unmanned aerial vehicles: Demonstration and study cases. In *Hybrid Technologies for Power Generation*; Elsevier: Amsterdam, The Netherlands, 2022; pp. 439–473.
34. Ye, X.; Savvarisal, A.; Tsourdos, A.; Zhang, D.; Jason, G. Review of hybrid electric powered aircraft, its conceptual design and energy management methodologies. *Chin. J. Aeronaut.* **2021**, *34*, 432–450.
35. Pan, Z.; An, L.; Wen, C. Recent advances in fuel cells based propulsion systems for unmanned aerial vehicles. *Appl. Energy* **2019**, *240*, 473–485. [[CrossRef](#)]
36. Li, S.; Gu, C.; Zhao, P.; Cheng, S. A novel hybrid propulsion system configuration and power distribution strategy for light electric aircraft. *Energy Convers. Manag.* **2021**, *238*, 114171. [[CrossRef](#)]
37. Xie, Y.; Savvaris, A.; Tsourdos, A. Fuzzy logic based equivalent consumption optimization of a hybrid electric propulsion system for unmanned aerial vehicles. *Aerosp. Sci. Technol.* **2019**, *85*, 13–23. [[CrossRef](#)]
38. Julier, S.J.; Uhlmann, J.K. Unscented filtering and nonlinear estimation. *Proc. IEEE* **2004**, *92*, 401–422. [[CrossRef](#)]
39. Yu, M.; Lan, D.; Huang, Y.; Wang, H.; Jiang, C.; Zhao, L. Event-based sequential prognosis for uncertain hybrid systems with intermittent faults. *IEEE Trans. Ind. Inform.* **2018**, *15*, 4455–4468. [[CrossRef](#)]
40. Yi, S.; Zorzi, M. Robust kalman filtering under model uncertainty: The case of degenerate densities. *IEEE Trans. Autom. Control* **2021**, *67*, 3458–3471. [[CrossRef](#)]
41. He, H.; Qin, H.; Sun, X.; Shui, Y. Comparison study on the battery SoC estimation with EKF and UKF algorithms. *Energies* **2013**, *6*, 5088–5100. [[CrossRef](#)]
42. Zhang, X.; Wu, J.; Kang, G. SOC Estimation of Lithium Battery by UKF Algorithm Based on Dynamic Parameter Model. In Proceedings of the 2016 13th International Conference on Ubiquitous Robots and Ambient Intelligence (URAI), Xi'an, China, 19–22 August 2016; IEEE: Manhattan, NY, USA, 2016; pp. 945–950.
43. Huang, C.; Yu, X.; Wang, Y.; Zhou, Y.; Li, R. State of charge estimation of li-ion batteries based on the noise-adaptive interacting multiple model. *Energy Rep.* **2021**, *7*, 8152–8161. [[CrossRef](#)]
44. He, Z.; Li, Y.; Sun, Y.; Zhao, S.; Lin, C.; Pan, C.; Wang, L. State-of-charge estimation of lithium ion batteries based on adaptive iterative extended Kalman filter. *J. Energy Storage* **2021**, *39*, 102593. [[CrossRef](#)]

Disclaimer/Publisher's Note: The statements, opinions and data contained in all publications are solely those of the individual author(s) and contributor(s) and not of MDPI and/or the editor(s). MDPI and/or the editor(s) disclaim responsibility for any injury to people or property resulting from any ideas, methods, instructions or products referred to in the content.